Journal of the Australian Ceramic Society
https://doi.org/10.1007/s41779-023-00927-2

RESEARCH

Effects of temperature and pH on the synthesis of nanohydroxyapatite powders by chemical precipitation

Gizem Mahmutoglu[1] · Aysenur Topsakal[2] · Eray Altan[2,3] · Nilgun Kuskonmaz[1] · Sibel Daglilar[1] · Faik Nuzhet Oktar[2,4] · Gokce Erdemir[5] · Serap Erdem Kuruca[6] · Sibel Akyol[7] · Oguzhan Gunduz[2,3] · Besim Ben-Nissan[8]

Received: 2 November 2021 / Revised: 22 June 2023 / Accepted: 9 July 2023

Abstract
Bone tissue engineering is based on a comprehensive understanding of bone structure, bone mechanics, and biology. In order to create nanostructured hydroxyapatite powders with customized properties, many synthesis strategies such as wet chemical precipitation, sol-gel, hydrothermal, and biomimetic approaches have been intensively researched through the years. Calcium phosphate (CaP)-based ceramic nanoparticles, including hydroxyapatite (HAp), were synthesized by the chemical precipitation technique at pH ranges of 7 to 11 and different calcination temperatures of 600 to 1100 °C. The synthesized powders were characterized by several techniques, including scanning electron microscopy (SEM), Fourier transform infrared spectroscopy (FTIR), X-ray powder diffraction (XRD), energy dispersive X-ray analysis (EDX), and in vitro cell culture assays. The particle size analysis and zeta potential of these powders were also carried out using the dynamic light scattering (DLS) and laser Doppler electrophoresis methods. The results showed that the pH levels of 9 to 11 range and calcination temperatures of 600 to 800 °C were adequate for appropriate nanohydroxyapatite powder production using this method. The particle size of the nanohydroxyapatite was approximately 55 nm, although they were agglomerated after calcination. The biocompatibility tests demonstrated that these nanohydroxyapatite (nHAp) powders produced have appropriate cytocompatibility and can be used for bone graft production and other biomedical applications.

Keywords Bioceramics · Nanoparticles · Hydroxyapatite · Bone grafts · Wet chemical precipitation

Introduction

Bone tissue engineering is a field that involves the repair and the growth of bone and at certain conditions the complete and accelerated renewal of the damaged area of the injured tissue. Bone graft synthesis and related tissue engineering are some of the most important areas of orthopedic surgery. In 2017, there were over 22.3 million orthopedic operations worldwide which also required bone grafting surgery to repair significant critical size bone defects arising from various accidents and diseases (like tumor resection) [1]. The bone graft and substitutes market was valued at US$2.9

✉ Faik Nuzhet Oktar
foktar@marmara.edu.tr

✉ Oguzhan Gunduz
ucemogu@ucl.ac.uk

✉ Besim Ben-Nissan
besim77@gmail.com

[1] Department of Metallurgical and Materials Engineering, Faculty of Chemical and Metallurgical Engineering, Yildiz Technical University, Istanbul, Turkey

[2] Center for Nanotechnology and Biomaterials Research, Marmara University, Marmara, Turkey

[3] Department of Metallurgical and Materials Engineering, Faculty of Technology, Marmara University, Marmara, Turkey

[4] Department of Bioengineering, Faculty of Engineering, Marmara University, Marmara, Turkey

[5] Department of Molecular Medicine, Aziz Sancar Institute of Experimental Medicine, Istanbul University, 34452 Istanbul, Turkey

[6] Department of Physiology, Faculty of Medicine, Istanbul University, 34452 Istanbul, Turkey

[7] Department of Physiology, Istanbul University-Cerrahpasa, Istanbul, Turkey

[8] School of Life Sciences, Faculty of Science, University of Technology, Sydney, NSW, Australia

Published online: 07 August 2023

Billion in 2019 and was projected to reach US$4.4 billion by 2027. The strategy in bone tissue engineering is based on pure calcium phosphates or composites made with two or more elements and bone substitute materials. The point of creating a composite is to combine the benefits of each component and add pharmaceuticals that can accelerate bone growth or their bioactivity. Kneser et al. [2] stated that the key issue in bone tissue engineering, which aims to produce or repair natural tissue, is to mimic the bone structure and its regeneration. Over the last two decades, many bone substitutes have been extensively researched and commercialized, including bioactive glasses, bioactive ceramics, and natural or synthetic polymers and their composites [3]. To create nHA powders with enhanced characteristics, researchers have investigated novel techniques such microwave-assisted synthesis [4], electrospinning [5], and sonochemical methods [6]. With the help of these methods, high-quality nHA powders can be created with improved reaction kinetics, shorter syntheses, and better control over particle properties. Although strictly speaking not fully true, HAp, with its chemical formula $Ca_{10}(PO_4)_6(OH)_2$, is widely accepted as the main inorganic component of bone and teeth [7–9]. In addition to the main component, the structure of bone contains a number of substitutional elements and components such as Mg, Sr, Si, Zn, and others. HAp ceramics have been well recorded that they are biocompatible and do not exhibit any cytotoxic effects [10]. HAp provides excellent biocompatibility and bioactivity within hard tissues and skin and muscle tissues. Bioactivity, as a definition, is given as "the ability of an implant or graft to create a chemical bond with the bone tissue" [11]. The applications of HAp powders have expanded across diverse fields. HAp has shown promise in the fields of bone tissue engineering, drug delivery systems, and dental restoration [12].

HAp bone grafts are produced as in high density or as interconnected porous structure materials. Porous HAp is an excellent material due to the interconnected pores that allow both mechanical interlock and direct bond to bone [9, 13], and it has excellent bioactivity despite its restricted use in long bones under load-bearing conditions because of its low strength and brittle structure due to the inherent porous structure [13, 14]. The synthetic HAp can be produced by various processing routes, including precipitation, sol-gel, and hydrothermal processing [9, 15–17]. In all these methods, the pH level during synthesis and the applied calcination and then sintering temperatures influences many properties of the final product. In this current study, we used a chemical precipitation method, and the reasons for this method are they can be carried out at room temperature and obtain a pure product at a reasonable cost [17]. This investigation is aimed to produce pure nano-sized HAp at different pH levels and calcination temperatures by a specific chemical precipitation method. Calcium phosphates according to their Ca to PO_4 ratio can be classified to include a number of different phases with different solubilities. In our previous study, calcium phosphate materials such as tri calcium phosphate, monetite, hydroxypatite, and whitlockite were successfully produced by mechano-chemical precipitation method. Acidic and basic environments were studied. Boskey and Posner stated the precipitation of calcium phosphate from a system which contains total calcium and phosphate each with a concentration higher than 10 milimoles per liter (mmol. l^{-1}) and at pH values greater than 6.8; the precipitation is always preceded by the formation of an amorphous precursor, hydroxyapatite (HAp) $Ca_5(PO_4)$ 3OH (10). This theory is very much consistent with the Ostwald rule of stages in precipitation. It was postulated that in this process there is transformation of precipitates through some intermediate states to the thermodynamically stable product, mainly a final HAp crystal [15, 17, 18].

It is thought that supersaturation, pH values, and impurities like magnesium and strontium are some of other factors that influence these transformations. [16]. It was postulated that carbonate environment in bone mineral enhanced IR shift of carbonate and stabilizes the non-apatitic surface layer present on apatite nanocrystals [17]. Theories have been suggested on the mechanisms of crystal formation; however, only a very few mechanisms have been globally accepted. Final morphologies and structures observed from these transformations are not clearly explained. The present work aims to explore the evolution of crystalline calcium phosphate, specifically HAp and their morphologies with respect to different pH environments and under different reaction temperatures. The difference in the study is that it examines the pH and calcination temperature range more broadly than the studies in the literature. The contribution and novelty of this present study is the examination of the synthesis parameters such as pH and calcination temperatures and the physicochemical analysis and the in vitro analysis such as cytotoxicity of the successful pure HAp produced.

Experimental procedures

Materials and methods

Although chemical and mechano-chemical methods were previously reported [18], the reaction of formation was investigated under a specific time intervals during the first 30 min, and the resultant changing pH levels during this transition periods were recorded. However, in this current work, we investigate the synthesis of pure nanohydroxyapatite (nHAp) formation by chemical precipitation method under different pH

conditions to determine the most appropriate pH, which ranged from 7 to 11 and the calcination temperatures of 600 to 1100 °C were investigated. It is well accepted that medically used calcium phosphate compounds have a Ca/P molar ratio ranging from 1.50 to 1.9. One of the primary purposes of this current work was to obtain pure nano HAp with a stoichiometric ratio of 1.67 by this method. Characterization of the products was carried out with several physicochemical methods. In addition, in vitro studies for cytotoxicity were also utilized for the determination of bioactivity and cytotoxicity.

Powder synthesis

Calcium nitrate tetrahydrate [$Ca(NO_3)_2{\cdot}4H_2O$], diammonium phosphate [$(NH_4)_2HPO_4$] powders and ammonia solution (25%) were obtained from Merck (Darmstadt, Germany). The Ca- and P-based solutions were prepared by dissolving 0.116 M $Ca(NO_3)_2{\cdot}4H_2O$ and 0.1 M $(NH_4)_2HPO_4$ separately in 200 mL distillate water. Two separate solutions were mixed in the magnetic stirrer for 30 min to obtain homogenous mixtures. The $(NH_4)_2HPO_4$ solution was then added slowly dropwise to the stirred solution, allowing the chemical reaction of the components to take place at a constant temperature (room temperature) with continuous stirring (60 min and 200−600 rpm). Because of the solutions were mixed by dropping, rpm was low as the reaction took place, and then, it was increased. After adding the $(NH_4)_2HPO_4$, this solution was adjusted to different pH levels by adding the ammonia solution to adjust the pH values of 7, 8, 9, 10, and 11, which were maintained during the experiment by adding additional ammonia solutions. Mixing was continued for 5 h by controlling the temperature and pH. When the mixing process was completed, a white precipitate was observed at the bottom of the precipitation beaker. This white powder was retained for Ostwald ripening in the solution used overnight foraging and growth. In this way, reactants had fully matured, and the Ca/P molar ratio was reached specific ratios, including the stoichiometric value of 1.67 for pure HAp [19–23]. The final powders produced were vacuum filtered after this maturation step. Using the distilled water several times, the NH_4NO_3 salts formed during the reaction were removed, and the resulting cake was dried in the oven at 90 °C for 12 h. In addition to this, one of the mixtures produced at pH = 11 was dried in the oven at 60 °C for additional 12 h. The dried powders were crushed to fine particle size by mortar and pestle to reduce or eliminate the agglomeration. Five new batches were derived from the powders by individual calcination temperatures in the ranges of 600, 700, 800, 900, 1000, and 1100 °C, which were retained for 2 h in the furnace. The furnace was heated to the target temperature and cooled down to room temperature with a 10 °C/min heating rate.

Characterization

Fourier transform infrared

Infrared spectra were recorded by Fourier transform infrared (FTIR) spectrometer (Jasco, FT/IR 4700, Jasco Inc., USA) equipped with Gladi attenuated total reflection (ATR) viewing plate (Diamond ATR crystal), and liquid-nitrogen cooled mercury cadmium telluride (MCT) detector at 500–4000 cm^{-1} wavenumber region.

Scanning electron microscope (SEM)

The morphology of the synthesized powders was obtained under scanning electron microscopy. Samples were coated with gold palladium for 160 s using a sputter. The SEM pictures were taken with EVA MA 10, ZEISS, USA, Supra 55VP SEM with RAITH E-beam lithography system and EBSD for the secondary electron imaging (SEI). The energy was kept at 20 kV, and working distance and magnification were varied to obtain the best possible images. The powder samples were fixed by mutual conductive adhesive tape on aluminum substrates and coated with gold-palladium using a sputter coater (CEA 010, Balzers union FL-9496 Balzers, SCD 020.)

Crystallography and composition

(a) SEM was coupled with EDX for observing the chemical composition of CaP based powders EDX with appropriate standards, and the numerical data recorded was used to calculate the Ca/P ratio of the powders. (b) X-ray diffraction (XRD) analysis was performed using an X-ray diffraction device (SHIMADZU XRD-6100, Shimadzu, Japan) to determine the crystal structures of the nanopowders at pH = 11 600 °C, 800 °C, and pH = 900 °C. The diffraction pattern was recorded in the 0.02 step size and the range of 2θ = 10 °-60 with a step time of 0.5 s °. CuKα radiation (λ = 0.15418 nm) was utilized. For the phase analysis of the products, the powder samples were loaded into an aluminum holder and flattened before analysis. The phase quantification was done using "Xpowder 12" software on full profile quantitative analysis of components using "Dirac" patterns and convolution and PIR scale factor.

Particle size analysis and zeta potential

The particle size and zeta potential of synthesized CaP-based powders were measured using dynamic light scattering (Horiba SZ-100, Korea) and laser Doppler electrophoresis method.

In vitro investigation with SAOS-2 cells

In vitro biocompatibility of the produced powders was investigated by two methods: (1) MTT assay to determine whether toxic substances were released from the powders produced and (2) SEM investigations to show attachment and proliferation of the SAOS-2 cells on materials. The Saos-2 (human osteosarcoma) cell line was obtained from the American Type Culture Collection (ATCC). Cells were cultured in Dulbecco's modified Eagle medium (DMEM, Gibco) with 10% fetal bovine serum (FBS, Gibco) and 1% penicillin/streptomycin in a 5% CO_2 humidified air incubator, which was maintained at 37 °C. When the cells reached 80% of confluence, they were washed with sterile PBS and trypsinized with 0.25% Trypsin-EDTA for passaging and seeding each time. The cells were used in cytotoxicity tests and SEM investigations for proliferation.

MTT cytotoxicity assay

The conditioned medium was prepared to determine any toxic effect induced by possible ionic leach-out products from the powders into the medium. For this purpose, 5 mL fresh medium Dulbecco's modified eagle medium (DMEM) was added in tubes with 0.05 g of the nano HAp powders, which were kept in an incubator at 37 °C with air. The powders were retained in this conditioned medium and were

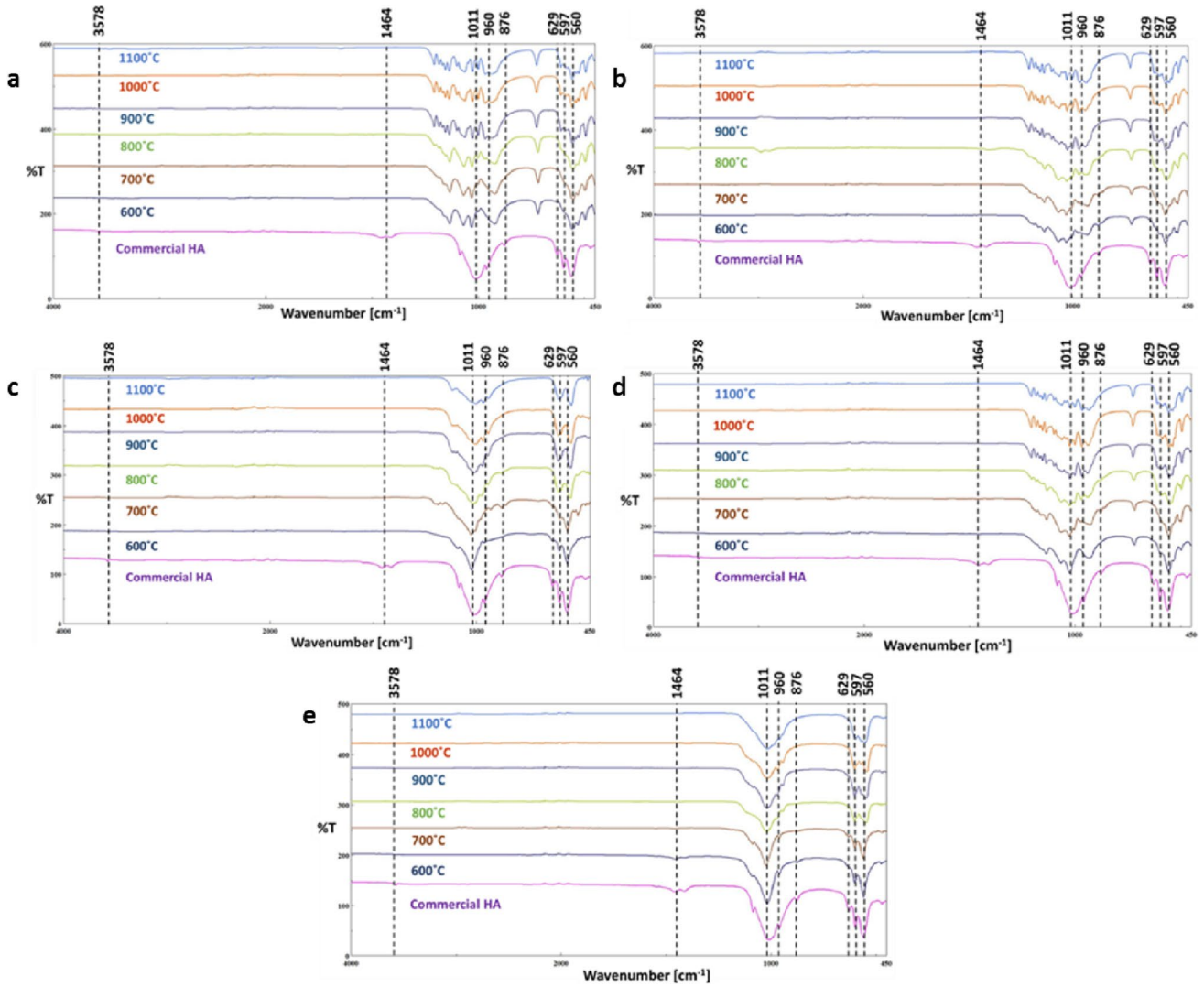

Fig. 1 The FT-IR spectra of HAp nanopowders sensitized at different pH levels, **a** pH = 7, **b** pH = 8, **c** pH = 9, **d** pH = 10, **e** pH = 11.

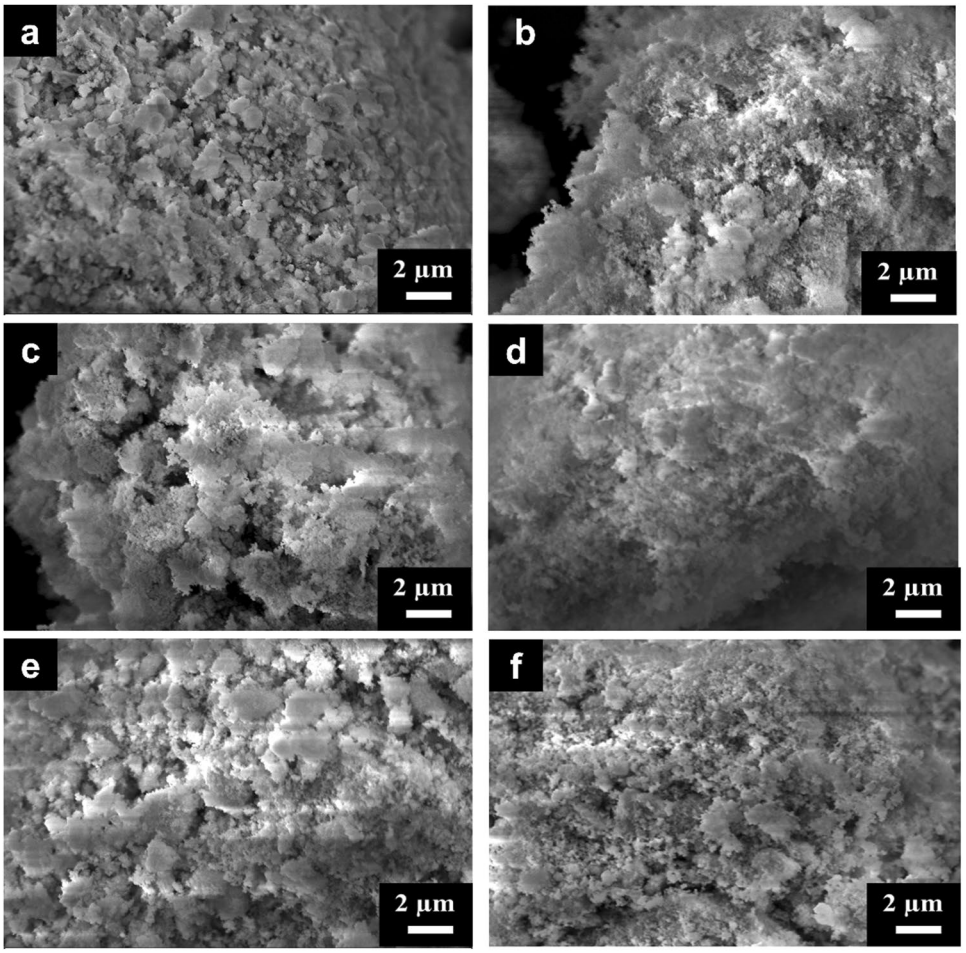

Fig. 2 SEM images collected at for different pH and calcination temperatures. **a** pH = 9 calcined at 600 °C, **b** pH = 9 calcined at 700 °C, **c** pH = 9 calcined at 800 °C, **d** pH = 11 calcined at 600 °C, **e** pH = 11 calcined at 700 °C, **f** pH = 11 calcined at 800 °C

extracted after the first, third, and seventh days and used in cytotoxicity tests. MTT assays were performed in 96-well plates. Saos-2 cells (about 10^5cells per well) were seeded onto the 4-h UV sterilized HAp, and 96-well plates incubated for 72 h. Cell viability was measured by determining mitochondrial NADH/NADHP–dependent dehydrogenase

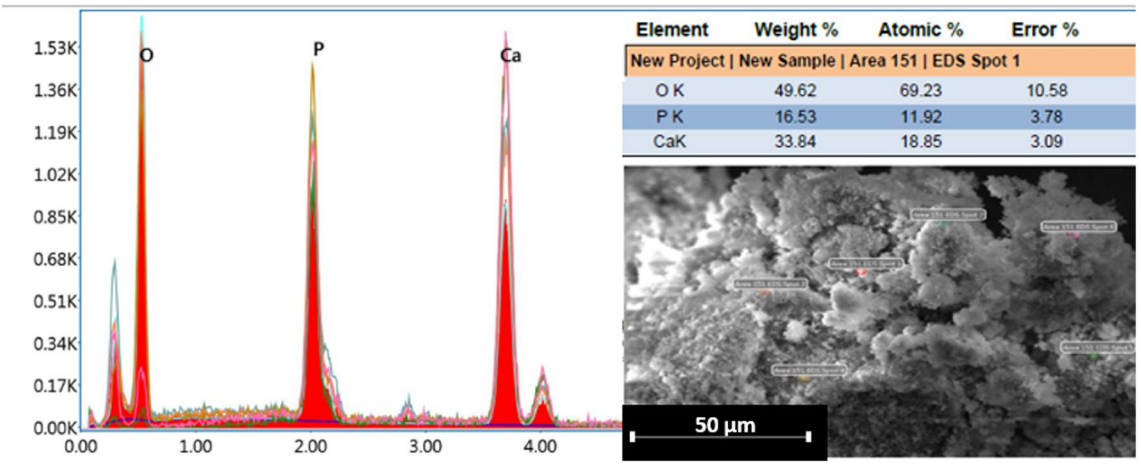

Fig. 3 SEM-EDX spectra of the CaP-based powders produced at pH = 11 and calcined at a temperature of 600 °C by chemical precipitation method

Table 1 EDX values from different points: (1) pH = 9 calcined at 600 °C, (2) pH = 9 calcined at 700 °C, (3) pH = 9 calcined at 800°C, (4) pH = 11 calcined at 600°C, (5) pH = 11 calcined at 700 °C, (6) pH = 11 calcined at 800 °C

Sample name	Spot one (Ca/P)	Spot two (Ca/P)	Average (Ca/P)
Exp. pH 9 – 600 °C	3.58	2.10	2.84 (± 0.23)
Exp. pH 9 – 700 °C	1.52	1.59	1.55 (± 0.27)
Exp. pH 9 – 800 °C	1.53	1.57	1.55 (± 0.21)
Exp. pH 11 – 600 °C	2.58	1.76	1.67 (± 0.22)
Exp. pH 11 – 700 °C	1.60	1.64	1.62 (± 0.21)
Exp. pH 11 – 800 °C	1.58	1.60	1.59 (± 0.28)

activity, which resulted in the cellular conversion of the 3-(4, 5-dimethylthiazol-2-gl)-5-(3-carboxymethyl phenyl)-2-(4-sulfophenyl-2H) tetrazolium salt into a soluble formazan dye. After 72 h, supernatants were removed, and 10 µL 3-{4, 5-dimethylthiazol-2yl}-2, 5-diphenyl-2H-tetrazolium-bromide (MTT, 5 mg/mL, Sigma) solution was added to each well. Following incubation at 37 °C for 3.5 h and kept dark in a humidified atmosphere at 5% CO_2 in the air, MTT was taken up by active cells and reduced in the mitochondria to insoluble purple formazan granules, according to Mossman study [23]. Subsequently, the supernatant was discarded, the precipitated formazan was dissolved in dimethyl sulfoxide (100 µL per well), and the optical density of the solution was evaluated using a microplate spectrophotometer (Kayto RT-2100 °C) at a wavelength of 570 nm. For the SEM cell culture investigations, the CaP-based powders were placed in the wells of 6-well cell culture plates and sterilized (By UV) for 4 h. Saos-2 cells (about 3×10^5cells per well) were seeded in these plastic dishes and incubated for 24 h in a humidified incubator at 37 °C with 95% air and 5% CO_2. At the end of 24 h, the media were removed, and specimens were fixed with a 3% volume fraction of glutaraldehyde, subjected to graded (30–100%) alcohol dehydration and kept at – 20 °C.

Table 2 Particle size analysis and zeta potential values of the powders synthesize

Sample name	Mean size (nm)*	Zeta potential (Mv)
Exp. pH 9 – 600 °C	179.9 (± 0.49)	– 48.5 (± 0.81)
Exp. pH 9 – 700 °C	239.8 (± 0.51)	– 58.3 (± 0.83)
Exp. pH 9 – 800 °C	133.1 (± 0.53)	– 62.6 (± 0.86)
Exp. pH 11 – 600 °C	87.6 (± 0.49)	– 47.8 (± 0.82)
Exp. pH 11 – 700 °C	113.5 (± 0.52)	– 72.0 (± 0.86)
Exp. pH 11 – 800 °C	55.6 (± 0.54)	– 46.3 (± 0.81)
Exp. pH 11 – green (not calcined)	142.6 (± 0.57)	– 30.0 (± 0.84)

*These are the values for the possibly agglomerated particles

Results and discussion

The powders produced were calcined at different temperatures and were analyzed using FT-IR spectroscopy (Fig. 1). Dotted lines represent functional groups associated with HAp [19, 20]. The bands for PO_4^{3-} and OH^- groups in the HAp can be identified at 560–597 cm^{-1} and 960–1011 cm^{-1} and were due to $(PO_4)^{3-}$. Depending on the literature [24], asymmetric stretching of $(PO_4)^{3-}$ at around 1041 cm^{-1} is specific peaks of HA. But 1000–1250 cm^{-1} bands did not indicate the specificity of HA. For the OH^- group, the bands positions are 629 cm^{-1} and 3578 cm^{-1}. The bands seen in 1464 cm^{-1} represent $(CO_3)^{2-}$. The results confirm the presence of calcium phosphate in the products by characteristic vibrations of the PO_4 tetrahedral ($\nu 1$ occurs at 962 cm^{-1} and

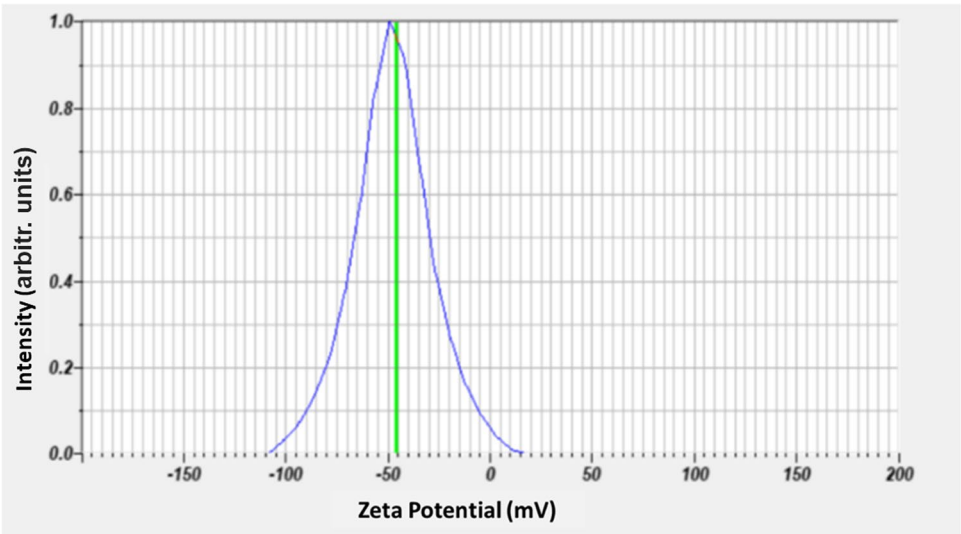

Fig. 4 Zeta potential graph analysis of the synthesized powder at pH = 11 and calcined at 600 °C

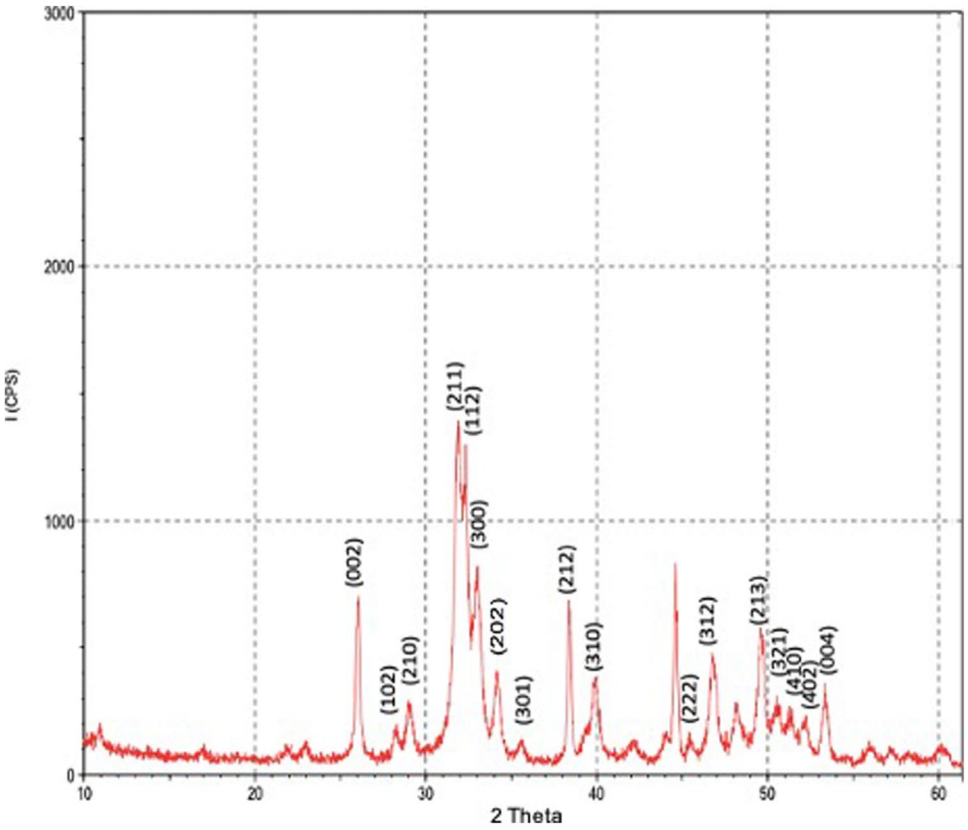

Fig. 5 XRD pattern of the synthesized powders at pH = 11 and calcined at 600 °C.

$\nu 2$ occurs at 470 cm^{-1}; $\nu 3$ occurs at 1047 cm^{-1} and 1087 cm^{-1}; $\nu 4$ occurs at 601 cm^{-1} and 571 cm^{-1}). These IR bands observed were matching very well with those reported in previous literature [17, 25, 26].

The substances synthesized under different conditions contain the characteristic bands corresponding to the groups $(PO_4)^{-3}$ and OH^-. Most of the bands observed match well with the pure HAp, specifically at pH 9 and pH 11 fired at 600 °C. However, the pH 7, 8, and 10 results had extra bands. Produced HA had the same properties with commercial HA. But, the pH 7, 8, and 10 results showed peak structures different from commercial HA. Some mentioned as impurities in the present FTIR spectrum have been observed and are irrelevant with the commercial HA FTIR peaks. The peaks that are compatible and overlapping with commercial HAp peaks were observed at lower temperatures of 600 °C, 700 °C, and 800 °C. TCP is formed when the temperature rises and the Ca/P ratio changes. The scanning electron microscope (SEM) was used for morphological analysis of the HAp powders at the same magnification (Fig. 2). Images show high agglomeration within each group. These agglomerates consist of very fine nanoparticles of hydroxyapatite at approximately 50 nm to 0.5 µm fine particles and agglomerates of up to 30 µm in size.

The standard EDX analysis was carried out on the CaP nanopowders (Fig. 3). The analysis revealed that calcium (Ca), phosphorus (P), and oxygen were the main constituents of these CaP-based powders. Besides all those, the Ca/P molar

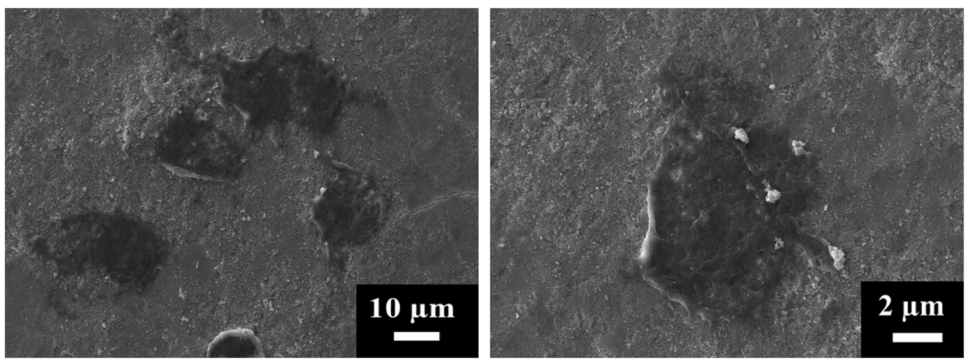

Fig. 6 SEM images collected at two magnifications of the HAp powders of pH = 11, 600 °C at 7th day of the cytotoxicity (MTT) tests showed no cytotoxicity

ratio of the elemental composition of different samples was also determined by using EDX. The calculated Ca/P molar ratio of the CaP-based powders, as shown in Table 1, ranges between 1.55 and 2.84. Among all these results, the Ca- based powders at pH = 11, which was calcined at 600 °C and 800 °C, have a Ca/P molar ratio of 1.67. This value is close to the Ca/P molar ratio of as carbonate hydroxyapatite [19].

HORIBA SZ-100Z nanoparticle analyzer, Korea, system has the dynamic light scattering (DLS) method to measure the size and the laser Doppler electrophoresis method for zeta potential measurement. This system can measure the size from 0.3 nm to 10 µm and the zeta potential value between − 500 and + 500 MV. There are three photomultiplier tube (PMT) detectors on this device. Laser diode light source is used at 532 nm and 10 mw power.

The device was scattered at 90 °C for the normal concentration samples and 173 °C for the high concentration samples. All samples were tested at 25 °C room temperature conditions. This specific size analyzer uses the reflected and refracted light from the falling powder particles within the solution to determine the particle size and their distribution according to their settlement rates (the DLS technique). The measured result indicates that at the pH = 11 treated at 800 °C, samples had the finest particle size powders at 55.6 nm, and their zeta potential was − 46.3 Mv. On the other hand, the pH = 11 at 600 °C had a particle size of 87.6 nm which is still finer than other groups investigated (Fig. 4). These results are in good agreement on our previous work on other calcium phosphate powders.

Laser Doppler electrophoresis [27] is used to determine the electrophoretic mobility of particles in suspensions in the solution. Zeta potential is the measurement of push or pull value between the particles [28]. The zeta potential is essential to understand the nanoparticle surface interactions and to estimate the stability of the nanoparticle in a solution [29]. Generally, nanoparticles greater than +30 mV or less than − 30mV have a high degree of stability [30, 31]. The zeta potential analysis of pH = 11 at 800 °C which exhibits approximately − 46.3 Mv shows the powder has relatively good stability. Similarly, the pH = 11 at 600 °C showed − 47.8, which also allows good stability (Table 2).

Characterization of the powders by XRD showed a straight baseline and sharp peaks of the diffractogram (Fig. 5). This confirmed that the product was well crystallized. XRD pattern showed that HAp was formed in pH = 11 treated at 600 °C, and no other traces of other calcium phosphates were detected. XRD template in Fig. 5 indicates that the structure of the CaP-based powders identified at that pH +11 level at 600 °C was similar to pure HAp JSPDS standard (9-0432) and showed a high match and consistency. In the XRD, no other impurities were detected, indicating that the main inorganic phase of the sample was the HAp crystal [31, 32].

The cytotoxicity (MTT) tests indicated that the synthesized powders (pH = 11 calcined at 600 °C) had no cytotoxicity

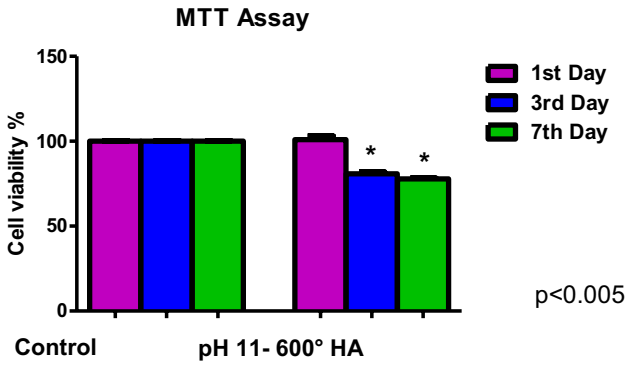

Fig. 7 MTT assay results of control and pH 11 – 600 °C HAp

compared to the control. On the first day of study, no changes in cell proliferation were observed on the third and seventh-day study, and a slight decrease in cell viability was detected (Fig. 7). Even if there is a decrease in MTT tests from day to day, vitality continues as seen in the 7th day SEM test. As it can be seen from the SEM images, the cells are viable and spread very easily (Fig. 6). The proliferation and growth are normal. The cell-scaffold interaction is indicated in Fig. 6. Statistically significant results are revealed by (*), and the p value was calculated by ANOVA analysis as $p < 0.005$.

Conclusions

CaP-based synthetic nanopowders of pure hydroxyapatite were successfully produced by the chemical precipitation method. However a high agglomeration after the drying and calcination was detected. During the process, nanopowders were synthesized at 5 different pH and 6 different calcination temperatures. During the tests, nanohydroxyapatite powders were successfully produced at pH 11 and calcination temperatures of 600 °C and at 800 °C. During FTIR analysis, PO_4^{3-}, OH^-, $(CO_3)^{2-}$ functional groups specific to HAp were identified. Biological apatites are carbonate apatites. In this current work, the observance of $(CO_3)^2$ in FTIR studies indicates a bone-like carbonate hydroxyapatite structure. SEM investigation showed that powders produced were microparticles that were highly agglomerated. The particle sizes were measured by the DLS method using the HORIBA particle size analyzer, and particle sizes as small as ~ 55 nm were achieved successfully. Therefore, it can be understood that desired particle sizes can be obtained. XRD analysis showed that the main inorganic phase was HAp with no other impurities for pH = 11 treated at 600 and 800 °C. It can be said that pure HAp can be produced without any other impurities. According to the EDX, the stoichiometric ratio of 1.67, the Ca/P ratio of commercially pure HAp, was successfully achieved. The in vitro studies exhibited that produced HAp can be used in medical and biomedical applications.

Cytotoxicity tests demonstrated that HAp has suitable cytocompatibility. Also the method used was simple and highly economical compared with other methods.

Acknowledgements The authors would like to thank to their all collaborators for their useful suggestions to improve this paper.

Data Availability The data that support the findings of this study are available from the corresponding author upon reasonable request.

Declarations

Conflict of interest The authors declare no competing interests.

References

1. Javaid, M.A., Kaartinen, M.T., Javaid, M.: Mesenchymal stem cell-based bone tissue engineering. International Dental Journal of Students Res. **1**, 24–35 (2012)
2. Kneser, U., Schaefer, D.J., Polykandriotis, E., Horch, R.E.: Tissue engineering of bone: the reconstructive surgeon's point of view. J. Cell. Mol. Med. **10**(1), 7–19 (2006)
3. Cegla, R.-N.R., Macha, I.J., Ben-Nissan, B., Grossin, D., Heness, G., Chung, R.-J.: Comparative study of conversion of coral with ammonium dihydrogen phosphate and orthophosphoric acid to produce calcium phosphates. J. Aust. Ceram. **50**(2), 154–1561 (2014)
4. Li, S., Yang, F., Zheng, L., Liu, Y.: Microwave-assisted synthesis of hydroxyapatite nanoparticles: A review. J. Inorganic Mater. **36**(2), 141–154 (2021)
5. Gao, J., Wang, Z., Li, Y., Liu, Y., Zhu, X.: Recent advances in the synthesis of hydroxyapatite nanomaterials via electrospinning for biomedical applications. J. Biomater. Appl. **36**(2), 256–276 (2022)
6. Ravikumar, N., Zhu, W., Kamruddin, M.: Recent advances in sonochemical synthesis of hydroxyapatite nanoparticles: a comprehensive review. Ultrason. Sonochem. **86**, 105480 (2023)
7. Brown, P.W., Paul, W., Constantz, B.: Hydroxyapatite and related materials. CRC (1994)
8. Suchanek, W., Yoshimura, M.: Processing and properties of hydroxyapatite-based biomaterials for use as hard tissue replacement implants. J. Mater. Res. **13**(1), 94–117 (1998)
9. Peitl, O., Zanotto, E.D., Serbena, F.C., Hench, L.L.: Bioactive glass-ceramics for load-bearing applications. An Introduction to Bioceramics. 495–503 (2013)
10. Macha, I.J., Ozyegin, L.S., Chou, J., Samur, R., Oktar, F.N., Ben-Nissan, B.: An Alternative synthesis method for Di calcium phosphate (Monetite) powders from Mediterranean mussel (Mytilus galloprovincialis) Shells. J. Aust. Ceram. Soc. **49**(2), 122–128 (2013)
11. Vallet-Regí, M., González-Calbet, J.M.: Calcium phosphates as substitution of bone tissues. Prog. Solid State Chem. **32**(1–2), 1–31 (2004)
12. Yang, S., Jin, Y., Sun, H., Xing, Y., Wang, X.: Nanostructured hydroxyapatite-based biomaterials for bone tissue engineering: a review. J. Biomed. Mater. Res. A. **110**(1), 15–32 (2022)
13. Prokopiev, O., Sevostianov, I.: Dependence of the mechanical properties of sintered hydroxyapatite on the sintering temperature. Mater. Sci. Eng. A. **431**(1–2), 218–227 (2006)
14. LeGeros, R.Z.: Calcium phosphates in enamel, dentin and bone. Calcium Phospates in Oral Biology and Medicine. **15**, 108–129 (1991)
15. Boskey, A.L., Posner, A.S.: Conversion of amorphous calcium phosphate to microcrystalline hydroxyapatite. A pH-dependent, solution- mediated, solid-solid conversion. J. Phys. Chem. **77**(19), 2313–2317 (1973)
16. Ben-Nissan, B., Choi, A.H.: Calcium phosphate nanocoatings: production, physical and biological properties, and biomedical applications. Nanobioceramics for Healthcare Applications. 105–149 (2017)
17. Macha, I.J., Boonyang, U., Cazalbou, S., Ben-Nissan, B., Charvillat, C., Oktar, F.N., Grossin, D.: Comparative study of Coral Conversion, Part 2: Microstructural evolution of calcium phosphate. J. Aust. Ceram. Soc. (2015)
18. Eslami, H., Solati-Hashjin, M., Tahriri, M.: Synthesis and characterization of nano-hydroxyapatite (n-HAP) using the wet chemical technique. Int. J. Phys. Sci. **8**(32), 1639–1645 (2013)
19. Al-Qasas, N.S., Rohani, S.: Synthesis of pure hydroxyapatite and the effect of synthesis conditions on its yield, crystallinity, morphology and mean particle size. Sep. Sci. Technol. **40**(15), 3187–3224 (2005)
20. Jiang, S.D., Yao, Q.Z., Ma, Y.F., Zhou, G.T., Fu, S.Q.: Phosphate-dependent morphological evolution of hydroxyapatite and implication for biomineralization. Gondw. Res. **28**(2), 858–868 (2015)
21. Liu, Q., Huang, S., Matinlinna, J.P., Chen, Z., Pan, H.: Insight into biological apatite: physicochemical properties and preparation approaches. Biomed. Res. Int. (2013)
22. Mosmann, T.: Rapid colorimetric assay for cellular growth and survival: application to proliferation and cytotoxicity assays. J. Immunol. Methods. **65**(1–2), 55–63 (1983)
23. Eslami, H., Solati-Hashjin, M., Tahriri, M.: Synthesis and characterization of hydroxyapatite nanocrystals via chemical precipitation technique. Iranian Journal of Pharmaceutical Sciences. **4**(2), 127–134 (2008)
24. Rapacz-Kmita, A., Paluszkiewicz, C., Ślósarczyk, A., Paszkiewicz, Z.: FTIR and XRD investigations on the thermal stability of hydroxyapatite during hot pressing and pressureless sintering processes. J. Mol. Struct. **744**, 653–656 (2005)
25. Fuentes, G., Hernández, Y., Campos, Y., López, N., Rojas, M.L., Peón, E., Almirall, A., Delgado, J.A.: Composition influence on properties of acrylic composites loaded with synthetic hydroxyapatite. Lat. Am. Appl. Res. **38**(2), 105–112 (2008)
26. Smith, B.A., Ware, B.R.: Apparatus and methods for laser doppler electrophoresis. Contemporary Topics in Analytical and Clinical Chemistry. **2**, 29–54 (1978)
27. Miller, J.D., Yalamanchili, M.R., Kellar, J.J.: Surface charge of alkali halide particles as determined by laser-doppler electrophoresis. Langmuir. **8**(5), 1464–1469 (1992)
28. Ding, Z., Jiang, Y., Liu, X.: Nanoemulsions-based drug delivery for brain tumors. In: Nanotechnology-Based Targeted Drug Delivery Systems for Brain Tumors, pp. 327–358. Elsevier (2018)
29. Nimesh, S., Chandra, R., Gupta, N.: Advances in nanomedicine for the delivery of therapeutic nucleic acids. Woodhead Publishing. (2017)
30. Joseph, E., Singhvi, G.: Multifunctional nanocrystals for cancer therapy: a potential nanocarrier. In: In: Nanomaterials for Drug Delivery and Therapy. Elsevier (2019)
31. Wei, K., Wang, Y., Lai, C., Ning, C., Wu, D., Wu, G., Zhao, N., Chen, X., Ye, J.: Synthesis and characterization of hydroxyapatite nanobelts and nanoparticles. Mater. Lett. **59**, 2–3 (2005)
32. Cengiz, B., Gokce, Y., Yildiz, N., Aktas, Z., Calimli, A.: Synthesis and characterization of hydroxyapatite nanoparticles. Colloids Surf. A Physicochem. Eng. Asp. **322**(1–3), 29–33 (2008)